Non-dilatant brittle deformation and strength weakening of olivine gabbro due to hydration

Yuya Akamatsu, Kumpei Nagase, and Ikuo Katayama

Department of Earth and Planetary Systems Science, Hiroshima University, Hiroshima 739-8526, Japan

Key Points:

- The fracture strength of hydrated olivine gabbro is significantly less than that of gabbro.
- Brittle deformation of hydrated olivine gabbro is not associated with dilatancy.
- Strength weakening and non-dilatant brittle failure can result from shear cracking of hydrous phyllosilicates.

Corresponding author: Yuya Akamatsu, y-akamatsu@hiroshima-u.ac.jp

Abstract

To investigate the influence of hydration on brittle deformation of oceanic crustal rocks, we conducted triaxial deformation experiments on gabbroic rocks with various degrees of hydration. Additional experiments were performed on samples of serpentinite and serpentinized peridotite for comparison. Elastic wave velocities were measured during deformation to monitor the development of stress-induced cracks.

Hydrated olivine gabbros reached a maximum differential stress of 225–350 MPa, which was considerably less than that recorded for gabbros (∼450 MPa), but comparable to those for serpentinized ultramafic rocks (250–300 MPa). Elastic wave velocities of hydrated olivine gabbros were almost constant during deformation and did not show a marked decrease, even immediately prior to failure. This indicated that the deformation of hydrated olivine gabbro is not associated with the opening of the stress-induced axial cracks that are responsible for dilatancy and are commonly observed during deformation of crystalline rocks. Microstructural observations of the samples recovered after deformation showed crack damage to be highly localized to shear fracture zones with no trace of stress-induced crack opening, consistent with the absence of dilatancy. These data suggest that brittle deformation of hydrated olivine gabbro can be accommodated by the development of shear cracks in hydration minerals such as serpentine and chlorite, even when they are present in only small amounts. This leads to non-dilatant brittle deformation and a weakening of fracture strength, similar to that observed during deformation of serpentinized peridotite. Our results suggest that the brittle behavior of the oceanic crust may change considerably due to hydration.

1 Introduction

Oceanic plates often experience hydration due to water-rock interactions associated with various tectonic and magmatic processes at the seafloor. Hydrous phyllosilicates such as serpentine, which result from the hydration of mafic and ultramafic rocks, have unique physical, mechanical, and rheological properties (e.g., Moore & Lockner, 2004); therefore, hydration of the oceanic plates is a key influence on several aspects of geodynamic processes in various tectonic settings (Guillot et al., 2015).

Laboratory deformation experiments have shown that, in the brittle regime, serpentinite deforms without the stress-induced opening of cracks that is typically observed in deforming polycrystalline rocks, such as granite, because the failure occurs purely by shear cracking along the mechanically weak (001) cleavage plane of serpentine (Escartín et al., 1997). Since shear cracks do not involve any porosity change, the elastic wave velocity of serpentinite is insensitive to brittle failure (David et al., 2018), whereas that of granite systematically decreases during deformation, owing to the opening of cracks (Paterson & Wong, 2005). Escartín et al. (2001) conducted triaxial deformation experiments to quantify the effect of serpentinization on the mechanical properties of peridotite. They found that the presence of only ∼10% serpentine governs the mode of brittle deformation of peridotite, resulting in an absence of significant volume change during deformation and a decrease in fracture strength to that of serpentinite. Although the influence of hydration on the physical and mechanical properties of mantle rocks has been well investigated by previous deformation experiments, the effects of hydration on gabbroic crustal rocks have not yet been constrained. Gabbroic rocks containing hydrated olivine grains are commonly found in tectonic settings such as oceanic core complexes (e.g., Michibayashi et al., 2008; Suhr et al., 2008; Beard et al., 2009; Nozaka & Fryer, 2011), transform faults (e.g., Manning et al., 1996; Nozaka et al., 2017), and ophiolites (e.g., Korenaga & Kelemen, 1997; Kelemen et al., 2020). In addition, recent seismic surveys have observed low-velocity zones in the incoming plate at outer-rise regions, indicating that hydration occurs even to the depths of the uppermost mantle, owing to bending-related faulting (e.g., Ranero et al., 2003; Grevemeyer et al., 2007; Contreras-Reyes et al., 2008; Van Avendonk et al., 2011; Fujie et al., 2013; Shillington et al., 2015; Wan et al., 2019). Even a small amount of mechanically weak hydration minerals can drastically

change the rheological behavior of bulk rock; therefore, understanding the effect of hydration on gabbroic crustal rocks is essential for interpreting the mechanical behavior of the oceanic plate, and associated seismological signatures, where hydration occurs.

In this study, we performed triaxial deformation experiments on gabbros and olivine-bearing gabbros containing hydration minerals such as serpentine and chlorite, to investigate the influence of hydration on brittle deformation in crustal rocks. We compare the results to those of additional experiments conducted on serpentinite and serpentinized peridotite samples. Elastic wave velocities were measured during the deformation experiments to monitor the development of stress-induced cracks (e.g., Sayers & Kachanov, 1995; Schubnel et al., 2006; Fortin et al., 2011; Nicolas et al., 2016; David et al., 2018; Zaima & Katayama, 2018). We conclude by discussing the implications of our mechanical and velocity data for understanding the effects of hydration on the brittle behavior of the oceanic lithosphere.

2 Method

2.1 Sample descriptions

Deformation experiments were conducted on nine samples of varying lithology, including olivine gabbros, gabbros, serpentinized peridotite, and lizardite serpentinite. Representative micrographs of the experimental samples are shown in Figure 1. Gabbro samples (OM-10 and OM-17) were collected from the Samail ophiolite in Oman and are composed of plagioclase, clinopyroxene, and minor amounts of hornblende and epidote (Figure 1a, b). Olivine gabbro samples OG1, CM1A-113z, and OM-4 were also collected from the Samail ophiolite, and sample HK-25 was collected from the Horoman Complex in Japan. CM1A-113z is an olivine gabbro core sample recovered by the Oman Drilling Project, which sampled drill cores throughout the fossilized crust-mantle transition zone in the Samail ophiolite (Kelemen et al., 2020). These olivine gabbros consist mainly of plagioclase, clinopyroxene, and 15–36% of primary olivine. The olivine grains were variably hydrated, with serpentine and chlorite contents of between 6% and 27% (Table 1). In this study, we determined the hydration degree of olivine grains using petrographic analyses to calculate the ratio of primary olivine to serpentine and chlorite. Samples OM-4, CM1A-113z, and HK-25 have the olivine hydration degree of 44–75%, and the serpentine in these samples forms a mesh texture (Figure 1) that is indicative of low temperature serpentinization and is commonly observed in serpentinized peridotite. These samples are also characterized by fractures which are commonly filled with chlorite and connecting between hydrated olivine grains, which was possibly caused by volume expansion associated with olivine hydration (Yoshida et al., n.d.). Samples OG-1.1 and OG-1.2 have the olivine hydration degree of 56%, but no mesh texture is observed; however, some olivine grains show replacement by serpentine and chlorite along grain boundaries (Figure 1c), while others have undergone complete hydration and exhibit a pseudostratigraphy of serpentine and chlorite (Table 1). Serpentinized peridotite (ST-12) and lizardite serpentinite (MK7-05) samples were collected from the Samail ophiolite in Oman and the accretionary prism in the Mineoka Belt in Japan, respectively. These ultramafic rock samples are composed of primary olivine, orthopyroxene, lizardite, and chrysotile. The hydration (serpentinization) degree is estimated as 60% in ST-12 and 88% in MK7-05. The representative micrographs show serpentine mesh textures in both of these samples (Figure 1g, h).

The experimental samples were cored into cylinders of 20 mm in diameter and 40 mm in length, and the flat end surfaces ground parallel to within 0.01 mm. Sample densities and porosities were calculated from dry and wet masses at ambient conditions. All specimens were dried in an oven at 70°C for at least 24 hours prior to deformation experiments.

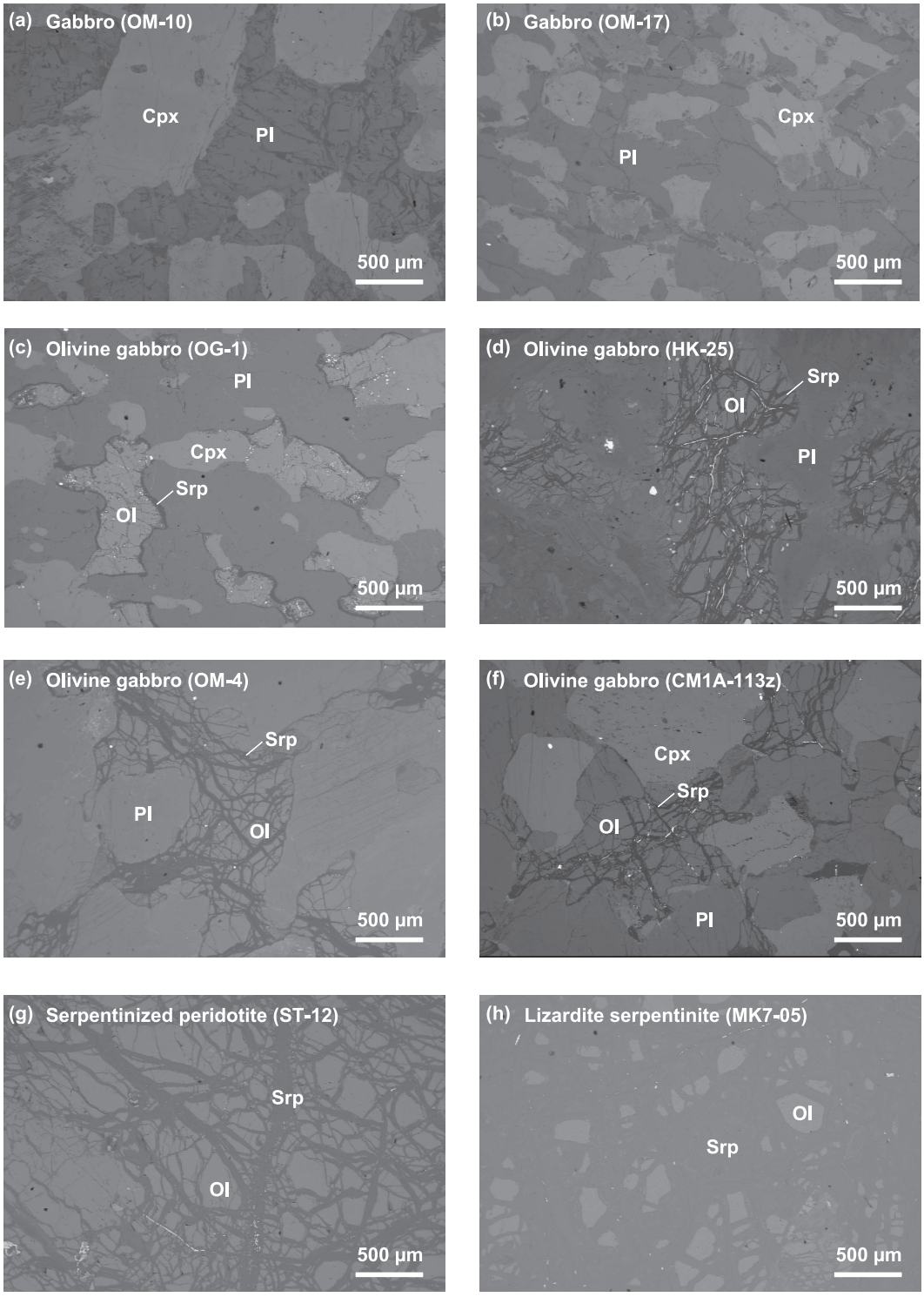

Figure 1. SEM images of each experimental sample: gabbro (a,b), olivine gabbro (c–f), serpentinized peridotite (g), and lizardite serpentinite (h). Abbriviations for minerals: Cpx, Clinopyroxene; Pl, Plagioclase; Ol, Olivine; Srp, Serpentine.

Table 1. Sample descriptions.

Sample	Rock type	Locality	Mineral content (%)		Olivine hydration degree (%)
			Ol	Srp	
OG-1.1	Olivine gabbro	Oman	7(15)	8[a]	56 ± 23
OG-1.2	Olivine gabbro	Oman	7(15)	8[a]	56 ± 23
CM1A-113z	Olivine gabbro	Oman	9(15)	6	44 ± 14
HK-25	Olivine gabbro	Horoman	9(36)	27	75 ± 12
OM-4	Olivine gabbro	Oman	9(22)	13	62 ± 17
OM-17	Gabbro	Oman	0	0	0
OM-10	Gabbro	Oman	0	0	0
ST-12	Serpentinized peridotite	Oman	40(100)[b]	60	60
MK7-05	Lizardite serpentinite	Mineoka	12(100)[b]	88	88

Abbreviations are corresponding to Figure 1.

The numbers inside parentheses show the estimated primary content (i.e., Ol + Srp).

Olivine hydration degree was determined by the ratio of primary olivine versus serpentine and chlorite.

[a] Chlorite content is included.

[b] Primary orthopyroxene content is included.

2.2 Experimental procedure

Triaxial deformation experiments were performed using the intra-vessel deformation and fluid flow apparatus at Hiroshima University; please see Zaima and Katayama (2018) for more detail about the apparatus. All experiments were conducted under dry conditions at a constant displacement rate of 0.002–0.003 mm/min (corresponding to an equivalent strain rate of $\sim 10^{-6} s^{-1}$), at room temperature, and with a confining pressure of 20 MPa. The confining pressure was set to a constant value using a servo-controlled system to compensate for the piston movement during deformation. Axial displacement was measured by the external displacement transducer, while differential stress was determined from the difference between the axial and confining pressure, with an accuracy of 0.5 MPa. A machine stiffness correction was applied to the axial displacement data to account for mechanical distortion during deformation. The mechanical parameters were recorded by a data logger at a sampling rate of 1 Hz. As our experimental apparatus was not equipped with a high-resolution feedback system, we focused on the evolution of elastic wave velocities approaching the maximum differential stress, but not during the post-failure processes. The sample was jacketed in a polyolefin tube and silicone to separate it from the oil confining medium.

Elastic wave velocities were measured with lead zirconate titanate piezoelectric transducers of resonant frequency 2 MHz, using a pulse transmission method. Both P-wave and S-wave velocity data were acquired along the direction normal to the loading axis. S-waves were polarized in the planes horizontal (SH-wave) and perpendicular (SV-wave) to the axis. An input pulse with an amplitude of 5 V and frequency of 2 MHz was sent to each transducer by a function generator, and the output signal was received by the remaining transducers and digitalized by an oscilloscope. The velocity was then determined by dividing the path length by the travel time. The error in ultrasonic velocities was estimated as $< 1\%$, which reflects the picking accuracy of wave arrival times and possible changes in propagation path length owing to sample dilation during deformation.

Table 2. Summary of experimental results.

Run No.	Sample	Rock type	Density (g/cm^3)	Initial porosity (%)	Maximum differential stress (MPa)
IVA1570	OG-1.1	Olivine gabbro	3.01	0.11	305
IVA1573	OG-1.2	Olivine gabbro	3.01	0.11	348
IVA1580	CM1A-113z	Olivine gabbro	2.98	0.05	225
IVA1608	HK-25	Olivine gabbro	3.01	0.46	302
IVA1626	OM-4	Olivine gabbro	2.86	0.08	344
IVA1624	OM-17	Gabbro	2.95	0.14	457
IVA1625	OM-10	Gabbro	2.97	0.24	440
IVA1602	ST-12	Serpentinized peridotite	2.93	0.49	257
IVA1609	MK7-05	Lizardite serpentinite	2.63	1.56	300

3 Results

3.1 Mechanical data

Figure 2 shows the mechanical data obtained from the deformation experiments, with differential stress plotted as a function of axial displacement (strain). The results of the experiments are summarized in Table 2. Maximum differential stresses of ∼450 MPa are recorded for the gabbro samples, which are comparable to those of granite deformed under similar conditions (Zaima & Katayama, 2018). Olivine gabbro samples with hydration mineral contents of 6%–27% yielded maximum differential stresses ranging from 225 to 348 MPa. These values are 20%–50% less than those of gabbros, but are similar to those of serpentinized peridotite and lizardite serpentinite (257–300 MPa).

Figure 3 shows the relationship between the maximum differential stress and the hydration mineral content for each sample. The strength of gabbroic rocks decreases abruptly at hydration mineral contents $\geq 6\%$. Beyond this threshold, the maximum differential stress of hydrated olivine gabbro decreases from values close to those of gabbro to those of lizardite serpentinite and serpentinized peridotite. Such weakening has also been reported to occur as a result of hydration in peridotite. Experiments by Escartín et al. (1997) found the strength of peridotite to be a strongly nonlinear function of serpentinization. They observed that the strength of peridotite with ∼10% serpentine was comparable to that of pure serpentinite, and were able to explain this strength reduction as a result of the accommodation of deformation by interconnected serpentine grains, which are substantially weaker than olivine. We observe a similar relationship to that of peridotite in our deformation experiments, which suggests that the strength reduction in gabbroic rocks occurs due to the presence of hydrous phyllosilicates such as serpentine and chlorite, which are produced during hydration of olivine.

3.2 Elastic wave velocity

During deformation of gabbro samples, the measured elastic wave velocities remained nearly constant as the differential stress increased to approximately two-thirds of its maximum value, but then began to decrease with increasing differential stress (Figure 4). Prior to failure, the velocities had decreased by up to 20% of their initial values. For S-waves, the decrease prior to failure was much larger in the horizontally polarized S-wave velocity V_{SH} than the vertically polarized S-wave velocity V_{SV}. The S-wave anisotropy A_S is calculated

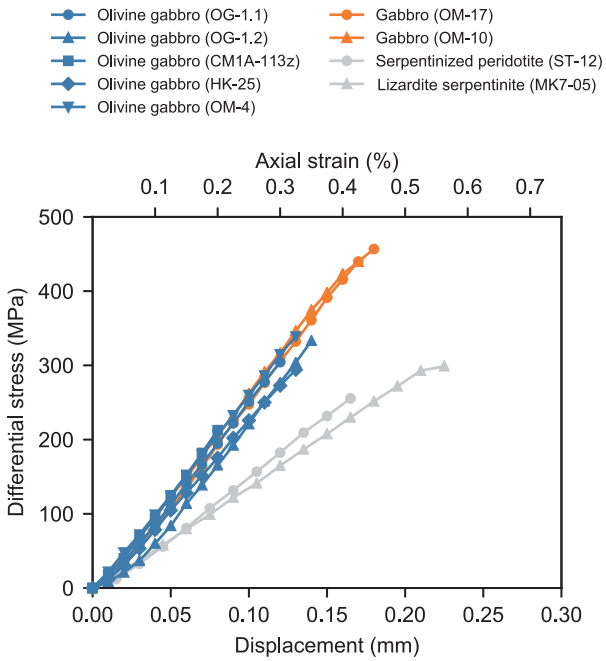

Figure 2. Mechanical data for each triaxial deformation experiment. Differential stress is plotted as a function of axial displacement. Axial strain, as inferred from displacement, is also shown on the upper axis.

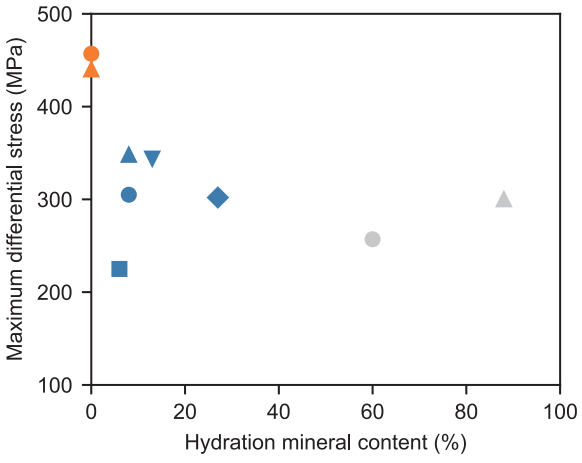

Figure 3. Relationship between the maximum differential stress and the hydration mineral content of each sample. Symbols and colors are the same as Figure 2.

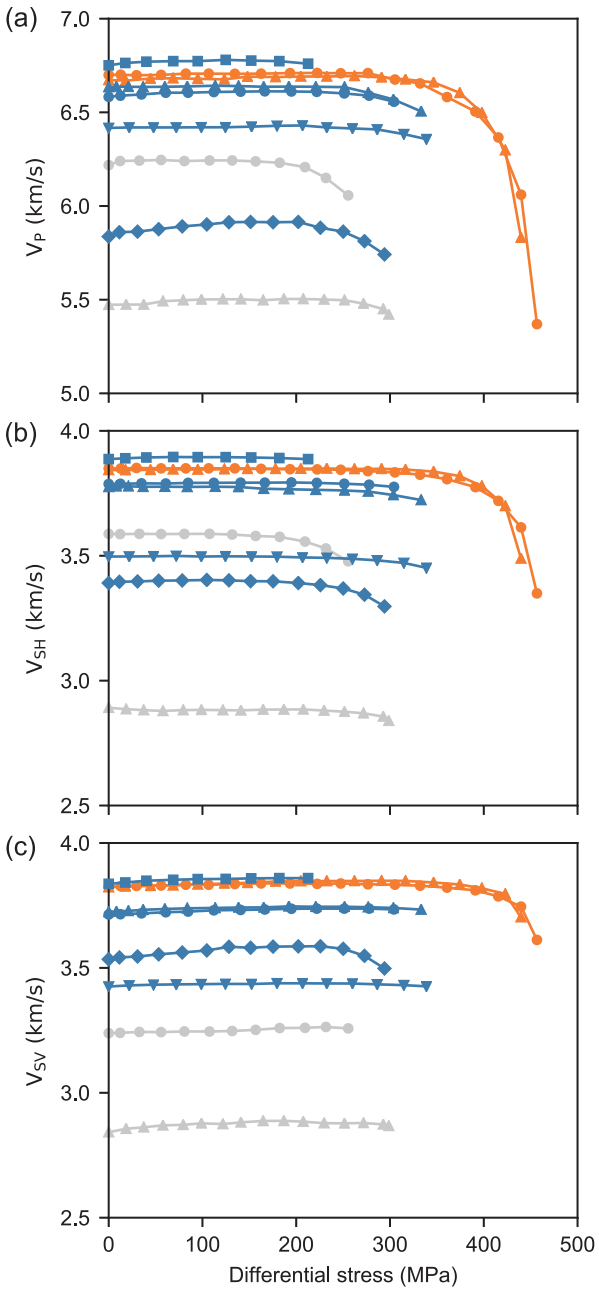

Figure 4. Elastic wave velocities recorded during deformation experiments. P- (a), SH- (b), and SV-wave (c) velocities are plotted as a function of differential stress. Symbols and colors are the same as in Figure 2.

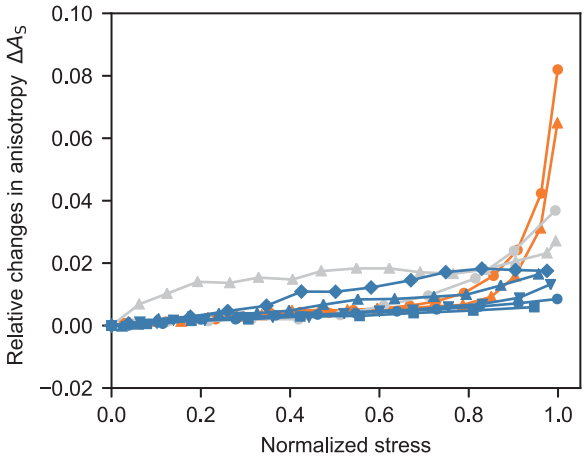

Figure 5. Relative changes in S-wave anisotropy during deformation experiments. Differential stress is normalized by the maximum differential stress in each sample. S-wave anisotropy was calculated as $(V_{SV} - V_{SH})/\bar{V_S}$, where $\bar{V_S} = (V_{SV} + V_{SH})/2$ (Wang et al., 2013). Symbols and colors are the same as Figure 2.

as:

$$A_S = \frac{V_{SV} - V_{SH}}{\bar{V_S}}, \tag{1}$$

where $\bar{V_S} = (V_{SV} + V_{SH})/2$ (Wang et al., 2013). The S-wave anisotropy in gabbro samples increased systematically as the samples approached failure (Figure 5). Similar changes in elastic wave velocities and anisotropy with deformation have been reported for a number of crystalline rocks, and are associated with the development of extensile cracks aligned with the axis of maximum compressive stress σ_1 (Lockner et al., 1977; Schubnel et al., 2006; Fortin et al., 2011; Nicolas et al., 2016; Zaima & Katayama, 2018).

In hydrated olivine gabbro samples, the elastic wave velocities remained almost constant during deformation, but decreased by a small amount ($< 3\%$) prior to failure(Figure 4). S-wave anisotropy increased slightly during deformation of the olivine gabbros, likely due to the closure of pre-existing cracks oriented perpendicular to σ_1. However, the changes in S-wave anisotropy were much less dramatic than those observed as the gabbro samples approached failure. Similar trends were observed for the serpentinite and serpentinized peridotite samples. Deformation in such serpentinized ultramafic rocks is not dilatant, as it is reportedly accommodated by shear cracking along the basal planes of serpentine, rather than through the opening of axial cracks (Escartín et al., 1997, 2001). The behavior of elastic wave velocities during deformation of hydrated olivine gabbros is similar to that of highly serpentinized peridotites, but markedly different to that of gabbros. This indicates that the brittle deformation of hydrated olivine gabbro is not related to typical crack development during deformation as well as hydrated peridotite.

3.3 Microstructure

Post-deformation, samples were recovered, impregnated with epoxy, and cut perpendicular to the fault zone to prepare polished thin sections for observation with a 15 kV scanning electron microscope (SEM). Figure 6 shows SEM images of typical microscale segments of the fault profile developed in each rock type. In these micrographs, the direction of axial compression is vertical. The gabbro samples show swarms of cracks oriented subparallel to the compression axis on both sides of the fractures (Figure 6a). This stress-induced axial cracking is consistent with the anisotropic changes in elastic wave velocities observed in

these samples during deformation (Figure 4) and with results from previously tested dilatant rocks. In hydrated olivine gabbro samples, crack damage is limited to the immediate vicinity of the fault zone. Areas away from the fault zone remain essentially undeformed and are indistinguishable from the pre-deformation material (Figure 6b). Macroscopic failure in the olivine gabbros appears to result from the sudden occurrence of one or more major fractures, as opposed to the propagation and coalescence of axial cracks that is commonly observed in crystalline rocks. SEM images of the serpentinized peridotite and serpentinite samples (Figure 6c, d) show similar features to those of the olivine gabbros. These observations are consistent with the absence of marked velocity changes recorded during deformation of the hydrated olivine gabbros and ultramafic rocks (Figure 4).

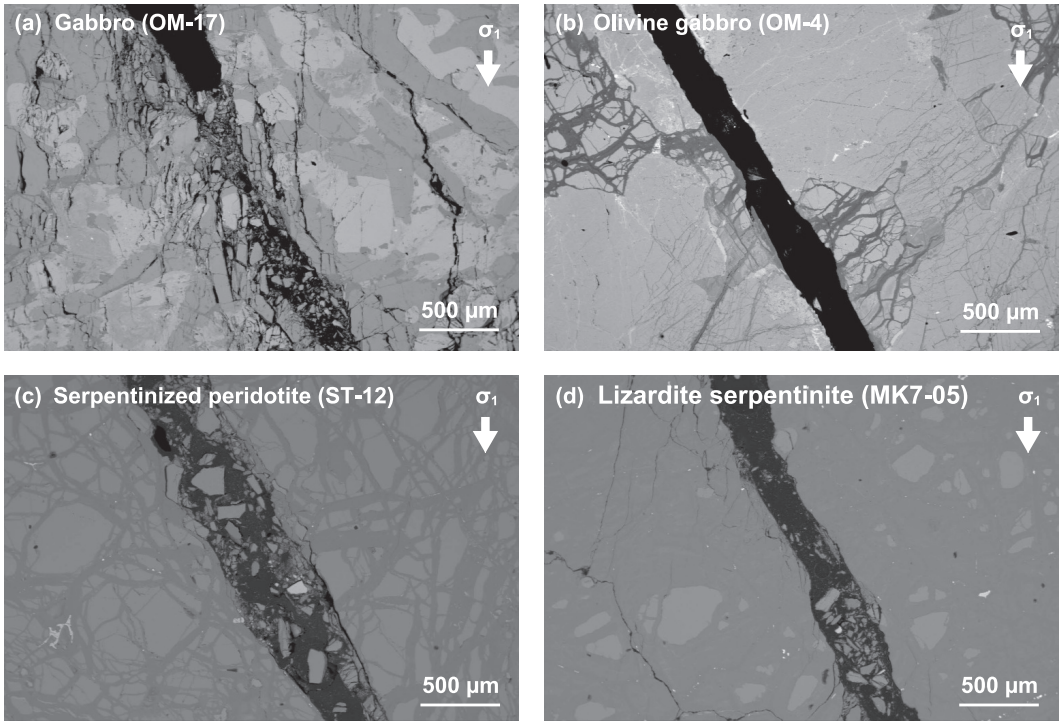

Figure 6. SEM images of fault planes in the failed samples recovered after deformation experiments: (a) gabbro, (b) olivine gabbro, (c) serpentinized peridotite, and (d) lizardite serpentinite. The loading axis (σ_1) is in the vertical direction.

4 Discussion

4.1 Non-dilatant brittle deformation of hydrated olivine gabbro

We observed no remarkable changes in elastic wave velocities during the brittle deformation of olivine gabbros with 6%–27% hydration minerals. In contrast, deformation in gabbro samples was characterized by a systematic decrease in wave velocities (Figures 4 and 5). In general, most crystalline rocks tend to exhibit significant volumetric dilation (termed dilatancy) during brittle deformation (Brace et al., 1966). A number of experimental studies have documented dilatancy to be caused by the opening of microcracks aligned subparallel to σ_1, prior to the formation of a macroscopic fault (e.g., Paterson & Wong, 2005). Since rock elasticity is closely related to the microstructure of pores, dilatant deformation results in a significant and anisotropic decrease in elastic wave velocities (e.g., Schubnel et al., 2006; Fortin et al., 2011; Nicolas et al., 2016; Zaima & Katayama, 2018). The absence of such

changes in elastic wave velocities during brittle deformation of hydrated olivine gabbros indicates that deformation in these rocks is not associated with typical dilatancy.

To quantify the amount of dilatancy, we inverted the measured elastic wave velocity to obtain the axial crack density, using the effective medium theory. When (x_1,x_2,x_3) represents orthogonal directions and x_3 is aligned with the loading axis, for a transversely isotropic medium, the elastic stiffness tensor component (i.e., P-wave modulus) in direction x_1, termed C_{11}, is related to P-wave velocity along the direction normal to the loading axis V_P as :

$$C_{11} = \rho V_\mathrm{P}^2, \tag{2}$$

where ρ is the density (Sayers & Kachanov, 1995). Assuming a medium containing randomly oriented penny-shaped cracks, parallel to the x_1x_2 plane, and with no interaction between individual cracks, the normalized elastic stiffness C_{11}/C_{11}^0 is given by (David et al., 2018):

$$\frac{C_{11}}{C_{11}^0} = 1 - \frac{32(1-2\nu_0+2\nu_0^2)}{3(2-\nu_0)(1-2\nu_0)}\gamma_{11}, \tag{3}$$

where γ_{11} is the crack density of cracks oriented parallel to the loading axis (i.e., the axial crack density), and C_{11}^0 and ν_0 are the reference P-wave modulus and Poisson's ratio of the crack-free matrix, respectively. Poisson's ratio ν is related to the elastic wave velocities by:

$$\nu = \frac{V_\mathrm{P}^2 - 2\bar{V_\mathrm{S}^2}}{2(V_\mathrm{P}^2 - \bar{V_\mathrm{S}^2})}. \tag{4}$$

For the reference parameters, we used initial values obtained before applying any differential stress; thus, our calculated crack densities represent relative changes during deformation. Since the direction x_2 is equivalent to x_1 for a transversely isotropic medium, the total crack density of axial cracks is given by: $\gamma = \gamma_{11} + \gamma_{22} = 2\gamma_{11}$. When cracks are assumed to be penny-shaped, the crack porosity added during deformation $\Delta\phi_\mathrm{c}$ can be expressed by:

$$\Delta\phi_\mathrm{c} = 2\pi\Delta\gamma\alpha, \tag{5}$$

where α is the crack aspect ratio. The amount of dilatancy is often considered equivalent to the crack porosity (Paterson & Wong, 2005); thus, here we quantify the amount of dilatancy $\Delta\varepsilon_\mathrm{v}$ as $\Delta\phi_\mathrm{c}$. Figure 7 shows the total axial crack density added during deformation and the corresponding amount of dilatancy, assuming $\alpha = 0.01$, which is a typical value for stress-induced cracks (Fortin et al., 2011). The amount of dilatancy calculated for gabbro samples ($\Delta\varepsilon_\mathrm{v}$=0.4%–0.6%, $\Delta\gamma$=0.06–0.09) is consistent with that observed in previously tested crystalline rocks (Escartín et al., 1997; Akamatsu et al., 2019). Hydrated olivine gabbros show almost no amounts of dilatancy (ε_v <0.1%, $\Delta\gamma$ <0.01), similar to the serpentinized ultramafic rocks, which are known to be non-dilatant during brittle deformation (Escartín et al., 1997, 2001). These results suggest that brittle failure in hydrated olivine gabbro is non-dilatant, and is instead characterized by the sudden occurrence of a main fault, without the development of pervasive axial cracks throughout the deformed sample (Figure 6).

Previous experimental studies have reported the non-dilatant brittle deformation of serpentine-bearing rocks. Escartín et al. (1997) found that highly foliated serpentinites do not exhibit dilatancy during brittle deformation, because the deformation is accommodated purely by shear cracks along the weak basal planes of serpentine, resulting in a negligible volume increase. Due to the absence of dilatancy, meanwhile, elastic wave velocities in antigorite have been observed to stay nearly unchanged during deformation, even immediately prior to brittle failure (David et al., 2018). A similar brittle behavior was observed in slightly serpentinized peridotite by Escartín et al. (2001). They observed that deformation in peridotite with only 10% lizardite and chrysotile was accommodated primarily by shear cracking in serpentine at stresses below those required for the nucleation of intragranular cracks within olivine, resulting in a non-dilatant mode of brittle deformation. These observations are consistent with the absence of remarkable changes in elastic wave velocities

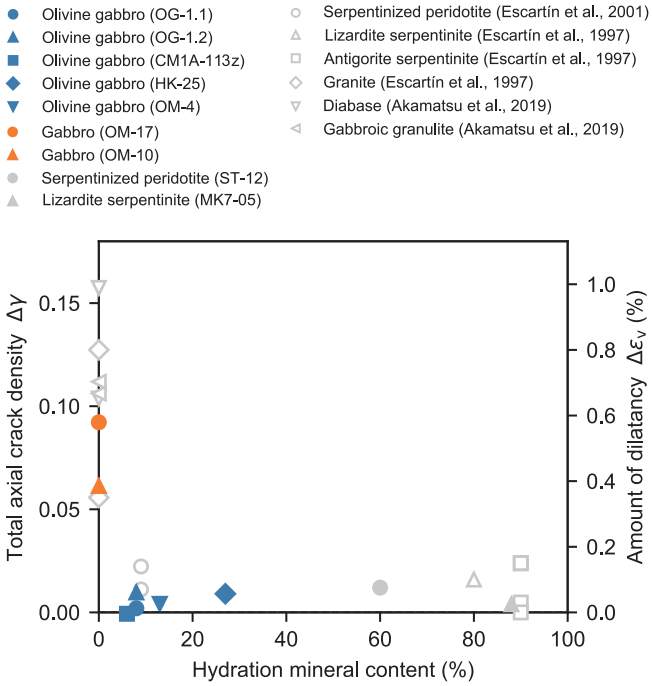

Figure 7. Relationship between the total axial crack density, amount of dilatancy, and hydration mineral content for each experimental sample. The total axial crack density was calculated using the effective medium theory (David et al., 2018). The amount of dilatancy was calculated from Equation 5, using an aspect ratio α of 0.01. Also plotted are experimental data for a range of dilatant and non-dilatant rocks reported by previous studies (Escartín et al., 1997, 2001; Akamatsu et al., 2019).

observed during the deformation of lizardite serpentinite (MK7-05) and 60% serpentinized peridotite (ST-12) in this study. The predominance of shear cracking in serpentine-bearing rocks has been supported quantitatively by measurements of fracture toughness K_{Ic}. K_{Ic} characterizes the stress required for the opening of axial "mode I" cracks, and has been shown to have a much higher value in antigorite serpentinite than in granite (David et al., 2020). This suggests that shear sliding is the favored mode of crack development in serpentine-bearing rocks. Based on interpretations from these previous studies, the absence of dilatancy during the deformation of our hydrated olivine gabbros can be explained if failure occurs from shear cracking in the hydrous phyllosilicates such as serpentine, rather than from extensile crack opening within the matrix minerals.

4.2 Strength weakening and deformation mechanism of hydrated olivine gabbro

In addition to the absence of stress-induced changes in elastic wave velocities during deformation, we observed that the strength of hydrated olivine gabbro was reduced to that of serpentinite and serpentinized peridotite, possibly as a result of hydration (Figure 3). Such a strength weakening has been reported for partially serpentinized peridotite by Escartín et al. (2001). They observed that the strength of peridotites decreased dramatically to that of pure serpentinite when the serpentinization degree exceeded ∼10%. They concluded that this weakening occurs because serpentine minerals interconnect along olivine grain boundaries and act as a weak phase, even at these low degrees of serpentinization. Meanwhile, Okazaki and Hirth (2020) conducted high-pressure triaxial deformation experiments on chlorite-

bearing mafic schists, and found that small amounts of chlorite could weaken the sample strength, in a similar manner to that suggested for serpentinized peridotite. Although we did observe that weakening correlated with hydration mineral content in our gabbro and hydrated olivine gabbro samples (Figure 3), SEM images showed that the serpentine and chlorite replacing olivine were not fully interconnected, because the primary olivine grains are well dispersed in these specimens (Figure 1).

In general, weak phases can dominate bulk rock behavior when present in minor quantities, providing they are well interconnected. If weak phases are well dispersed, the bulk deformation follows a mixing law (e.g., Tullis et al., 1991). Therefore, the mechanism of strength weakening in hydrated olivine gabbro can be somewhat different from that in peridotite. As peridotite is composed mainly of olivine, serpentine can interconnect sufficiently to weaken the bulk rock, even when present in small amounts. Our olivine gabbro samples on the other hand, contain only 15%–36% primary olivine, dispersed throughout the rock. However, in samples OM-4, CM1A-113z, and HK-25, cracks connecting between hydrated olivine grains are commonly observed. Theses fractures are possibly caused by reaction-induced volume expansion associated with hydration of olivine (Jamtveit et al., 2008) and commonly filled with chlorite (Yoshida et al., n.d.). Therefore, such crack-network could act as weak phases accommodating deformation as well as hydration minerals replacing olivine grains. In addition, given that their olivine hydration degrees are ranged between 44% and 75%, which is as high as those of serpentinized peridotite and serpentinite (60%–88%), the content and degree of hydration might be enough to reduce the brittle strength of gabbro, even for the samples with poor connectivity of hydration minerals such as OG-1. Our calculations of crack density, combined with microstructural observations of failed samples, demonstrate that formation of macroscopic fractures in hydrated olivine gabbro does not involve the development of significant axial "mode I" cracks (Figures 6 and 7). This indicates that shear cracking is favored over extensile crack opening, probably owing to the high K_{Ic} of serpentine (David et al., 2020), which might lead to the sudden propagation of shear cracks to form a macroscopic fault at lower stresses than those required for the brittle failure of gabbro.

Based on the experimental results, we suggest that the brittle failure of hydrated olivine gabbro and gabbro occurs by different mechanisms, as illustrated in Figure 8. According to previous studies, dilatant brittle failure is often interpreted in several stages (Scholz, 2019). In the initial stage of deformation, pre-existing cracks oriented at high angles to the loading direction are closed (stage I). This closure is associated with a slight increase in volumetric strain and elastic wave velocities, although these effects were not clearly observed in our samples, probably due to the low initial rock porosities (Table 2). Following stage I, the rock behaves as an elastic medium and the volumetric strain increases linearly with stress(stage II). At 30%–60% of the failure stress, cracks oriented subparallel to the loading direction begin to develop. This leads to a deviation from linearity in the stress–volumetric strain curve and a gradual decrease in elastic wave velocities (stage III). Finally, these cracks propagate and coalesce to form a macroscopic fracture zone, resulting in significant volume dilation and velocity reduction (stage IV).

While the gabbro samples exhibited typical dilatant deformation, the hydrated olivine gabbros appeared to deform by a different process, which we outline as follows: The initial stages of olivine gabbro deformation follow the previous framework; pre-existing cracks close (stage I) and the rock deforms elastically (stage II). However, the deformation is then accommodated primarily by shear cracking, likely along the weak basal planes of serpentine and chlorite, instead of by axial crack opening within the matrix minerals (stage III). As shear cracks do not create any void space, the stress–volumetric strain curve remains linear and the elastic wave velocities are not affected. This makes the differential stress at the onset of shear cracking difficult to detect. Therefore, we interpreted the development of shear cracks as stage III', which is indistinguishable to stage II. As the differential stress increases further, the unstable propagation of shear cracks suddenly occurs to form a localized fault

zone, identifiable by minor amounts of volume dilation and velocity reduction (stage IV). It is important to note that stage IV occurs at lower differential stress than is required for the failure of gabbro.

This study has focused on exploring the fundamental influence of hydration on the brittle deformation of gabbroic rocks but did not explore the pressure dependence of strength and dilatancy in hydrated olivine gabbro. Previous studies have shown the strength of serpentinites and serpentinized peridotites to increase with confining pressure until the onset of ductile deformation (at a confining pressure of 150–350 MPa), while the amount of dilatancy remains negligible (Escartín et al., 1997, 2001). The pressure dependence of strength is due to the increase in normal stress acting on crack surfaces altering the frictional resistance to shear cracking (David et al., 2018). Therefore, hydrated olivine gabbro may be expected to show a similar pressure dependence to that of serpentinite and serpentinized peridotite.

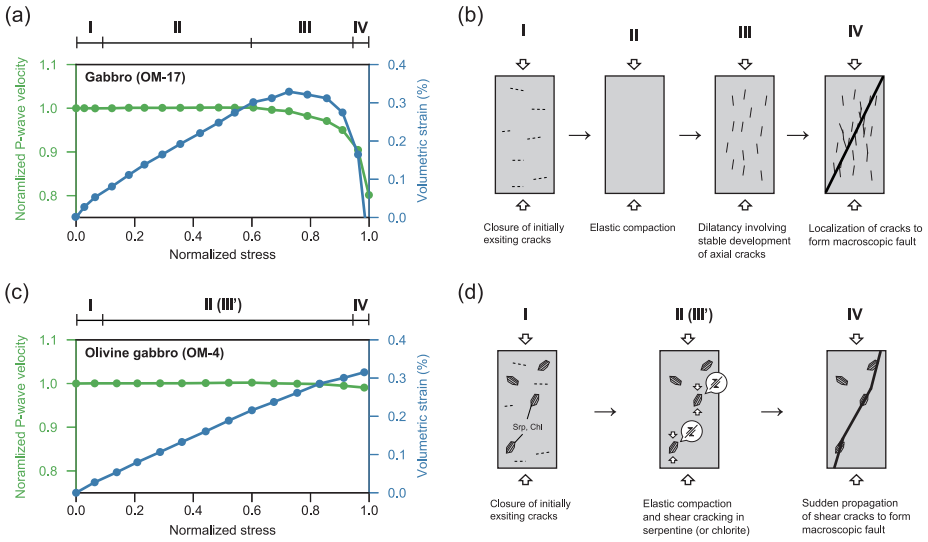

Figure 8. Ultrasonic and mechanical data with schematic diagrams showing the stages of brittle deformation for gabbro (OM-17) and hydrated olivine gabbro samples (OM-4). Normalized P-wave velocity, and volumetric strain estimated from calculated crack density, assuming the aspect ratio to be 0.01 are plotted against normalized differential stress (a, c). Schematic models of the brittle deformation mechanisms in gabbro and hydrated olivine gabbro (b, d). The onset of each stage of deformation in relation to the ultrasonic and mechanical data is shown at the top of (a) and (c), respectively.

4.3 Geophysical implications

Our experimental results suggest that the brittle and physical properties of the oceanic crust, which is comprised mainly of olivine-bearing gabbroic rocks, can be significantly changed as a result of hydration. The brittle strength of the oceanic crust can be reduced when the hydration minerals such as serpentine are present in only small amount. Brittle faulting of the natural environment is often assumed to involve pervasive crack formation around fault zones, consistent with the dilatant behavior usually observed during the deformation of crystalline rocks (e.g., Scholz et al., 1973). However, the absence of dilatancy during deformation of hydrated olivine gabbro indicates that brittle deformation in the hydrated oceanic crust may result in a crack-network entirely localized to the fault plane, as observed in our microstructural images of deformed samples (Figure 6b). The limited

porosity generation associated with this would prevent fluid flow in directions perpendicular to the fault planes.

In the mantle, water trapped within fault zones reacts readily with wall-rock peridotite by serpentinization. The formation of serpentine causes a volumetric expansion that enhances cracking (Jamtveit et al., 2008; Kelemen & Hirth, 2012). Serpentinization is geologically rapid at low temperatures (Macdonald & Fyfe, 1985), meaning that the supply of water to faults is the key control on the lateral extent of hydration in the mantle (Macdonald & Fyfe, 1985; Hatakeyama et al., 2017). In the oceanic crust, olivine is not the matrix mineral, meaning that less water is used in hydration reaction and less reaction-induced cracking occurs. We should note that recent numerical simulations suggested the reaction-induced cracking in the olivine-bearing gabbroic rocks to potentially enhance the background permeability by several order (Yoshida et al., n.d.). Nevertheless, the lateral fluid flow along cracks can be limited compared to the case in the mantle, and hydration could be confined to the vicinity of the fault zones.

The extent of hydration in the mantle is commonly inferred from seismic wave velocities, because the seismic wave velocity of peridotite decreases with serpentinization (Christensen, 2004). Seismic wave velocity is also dependent on the presence of cracks. Therefore, the effects of both hydration and porosity should be accounted for when interpreting the seismic structure of the oceanic mantle (Hatakeyama & Katayama, 2020). In contrast, seismic wave velocities in gabbroic rocks are not highly sensitive to alteration, meaning that porosity is usually the primary influence on seismic wave velocity in the oceanic crust (Korenaga, 2017). Our experimental data indicates that even slight hydration of the oceanic crust could inhibit the formation of crack networks during deformation, resulting in only minor changes in seismic wave velocities.

Hydration of the oceanic plate occurs primarily by hydrothermal circulation through fractures formed at spreading ridges. Fracturing in these areas is often confined to the upper part of the oceanic crust (see Faccenda (2014) for a review), meaning that hydration may not occur in the deeper part of the crust, where the olivine content is relatively high. However, gabbroic rocks containing hydrated olivine grains have been found in several settings. Such rocks have been sampled by seafloor drilling, dredging, and submersibles at tectonic windows, such as oceanic core complexes near slow-spreading ridges (e.g., Michibayashi et al., 2008; Suhr et al., 2008; Beard et al., 2009; Nozaka & Fryer, 2011) and transform faults near fast-spreading ridges (e.g., Manning et al., 1996; Nozaka et al., 2017). Hydrated olivine gabbros have also been commonly found at outcropping ophiolites (e.g., Korenaga & Kelemen, 1997; Kelemen et al., 2020). Since these fragments of the oceanic plate underwent hydration during and/or after the tectonic processes that caused their exposures, hydration of the oceanic crust might play a role in such tectonics. In addition, recent geophysical surveys have revealed that hydration occurs down to depths below the Moho due to water infiltration through bending-related faults, prior to subduction at outer-rise regions (e.g., Ranero et al., 2003; Grevemeyer et al., 2007; Contreras-Reyes et al., 2008; Van Avendonk et al., 2011; Key et al., 2012; Fujie et al., 2013; Shillington et al., 2015; Naif et al., 2015; Wan et al., 2019). Assuming failure is non-dilatant, we would expect only minor stress-induced crack damage around the bending-related faults. This could lead to a build-up of fluid pressure within the faults and a reduction in the effective confining pressure (i.e., lithostatic pressure) at a given depth, leading to rheological weakening of the faults in addition to the substantial weakening caused directly by hydration. Furthermore, the fault permeability would be increased, facilitating water penetration into the deeper parts of the oceanic plate.

Pressure and temperature at the depths of the lower oceanic crust are much higher than the conditions used in our experiments, but should be low enough that brittle deformation is dominant (McKenzie et al., 2005). Although care must be taken when applying low pressure and temperature experimental results to the oceanic crust, our results can provide new insights that aid the interpretation of geophysical data from the oceanic plates.

5 Conclusions

Triaxial deformation experiments were conducted on gabbroic rocks with various degrees of hydration, at room temperature and with a confining pressure of 20 MPa. Elastic wave velocities were measured during the deformation. While gabbros exhibited the typical dilatant behavior expected of crystalline rocks, hydrated olivine gabbros were characterized by weak fracture strength and the absence of dilatancy. These characteristics were consistent with microstructural observations in which hydrated olivine gabbros showed highly localized deformation structures with no trace of stress-induced axial crack opening. Our results suggest that the brittle deformation of hydrated olivine gabbro occurs by the development of shear cracks in mechanically weak hydrous phyllosilicates such as serpentine and chlorite. Our study indicates that the brittle behavior of the oceanic crust can be modified drastically by limited hydration.

Acknowledgments

We thank Prof. E. Takazawa at Niigata University and Dr. K. Hatakeyama at Hiroshima University for providing the outcrop samples collected from the Samail Ophiolite. We also thank Dr. N. Abe and Dr. K. Okazaki at JAMSTEC for providing the core sample by Oman Drilling Project. This study was supported by the Japan Society for the Promotion of Science (20H00200 and 20J22228). The data used in this study will eventually be available from Hiroshima University Institutional Repository.

References

Akamatsu, Y., Hatakeyama, K., & Katayama, I. (2019). Contrasting dilatant behaviors of mafic and ultramafic rocks based on triaxial deformation experiments. *Journal of Mineralogical and Petrological Sciences*, *114*(2), 79–86.

Beard, J. S., Frost, B. R., Fryer, P., McCaig, A., Searle, R., Ildefonse, B., ... Sharma, S. K. (2009). Onset and progression of serpentinization and magnetite formation in olivine-rich troctolite from iodp hole U1309D. *Journal of Petrology*, *50*(3), 387–403.

Brace, W., Paulding Jr, B., & Scholz, C. (1966). Dilatancy in the fracture of crystalline rocks. *Journal of Geophysical Research*, *71*(16), 3939–3953.

Christensen, N. I. (2004). Serpentinites, peridotites, and seismology. *International Geology Review*, *46*(9), 795–816.

Contreras-Reyes, E., Grevemeyer, I., Flueh, E. R., & Reichert, C. (2008). Upper lithospheric structure of the subduction zone offshore of southern arauco peninsula, chile, at 38 s. *Journal of Geophysical Research: Solid Earth*, *113*(B7).

David, E. C., Brantut, N., Hansen, L. N., & Mitchell, T. M. (2018). Absence of stress-induced anisotropy during brittle deformation in antigorite serpentinite. *Journal of Geophysical Research: Solid Earth*, *123*(12), 10–616.

David, E. C., Brantut, N., & Hirth, G. (2020). Sliding crack model for nonlinearity and hysteresis in the triaxial stress-strain curve of rock, and application to antigorite deformation. *Journal of Geophysical Research: Solid Earth*, *125*(10), e2019JB018970.

Escartín, J., Hirth, G., & Evans, B. (1997). Nondilatant brittle deformation of serpentinites: Implications for mohr-coulomb theory and the strength of faults. *Journal of Geophysical Research: Solid Earth*, *102*(B2), 2897–2913.

Escartín, J., Hirth, G., & Evans, B. (2001). Strength of slightly serpentinized peridotites: Implications for the tectonics of oceanic lithosphere. *Geology*, *29*(11), 1023–1026.

Faccenda, M. (2014). Water in the slab: A trilogy. *Tectonophysics*, *614*, 1–30.

Fortin, J., Stanchits, S., Vinciguerra, S., & Guéguen, Y. (2011). Influence of thermal and mechanical cracks on permeability and elastic wave velocities in a basalt from mt. etna volcano subjected to elevated pressure. *Tectonophysics*, *503*(1-2), 60–74.

Fujie, G., Kodaira, S., Yamashita, M., Sato, T., Takahashi, T., & Takahashi, N. (2013). Systematic changes in the incoming plate structure at the kuril trench. *Geophysical Research Letters*, *40*(1), 88–93.

Grevemeyer, I., Ranero, C. R., Flueh, E. R., Kläschen, D., & Bialas, J. (2007). Passive and active seismological study of bending-related faulting and mantle serpentinization at the middle america trench. *Earth and Planetary Science Letters*, *258*(3-4), 528–542.

Guillot, S., Schwartz, S., Reynard, B., Agard, P., & Prigent, C. (2015). Tectonic significance of serpentinites. *Tectonophysics*, *646*, 1–19.

Hatakeyama, K., & Katayama, I. (2020). Pore fluid effects on elastic wave velocities of serpentinite and implications for estimates of serpentinization in oceanic lithosphere. *Tectonophysics*, *775*, 228309.

Hatakeyama, K., Katayama, I., Hirauchi, K., & Michibayashi, K. (2017). Mantle hydration along outer-rise faults inferred from serpentinite permeability. *Scientific reports*, *7*(1), 1–8.

Jamtveit, B., Malthe-Sørenssen, A., & Kostenko, O. (2008). Reaction enhanced permeability during retrogressive metamorphism. *Earth and Planetary Science Letters*, *267*(3-4), 620–627.

Kelemen, P. B., & Hirth, G. (2012). Reaction-driven cracking during retrograde metamorphism: Olivine hydration and carbonation. *Earth and Planetary Science Letters*, *345*, 81–89.

Kelemen, P. B., Matter, J., Teagle, D., & Coggon, J. (2020). Proceedings of the oman drilling project.

Key, K., Constable, S., Matsuno, T., Evans, R. L., & Myer, D. (2012). Electromagnetic detection of plate hydration due to bending faults at the middle america trench. *Earth and Planetary Science Letters*, *351*, 45–53.

Korenaga, J. (2017). On the extent of mantle hydration caused by plate bending. *Earth and Planetary Science Letters*, *457*, 1–9.

Korenaga, J., & Kelemen, P. B. (1997). Origin of gabbro sills in the moho transition zone of the oman ophiolite: Implications for magma transport in the oceanic lower crust. *Journal of Geophysical Research: Solid Earth*, *102*(B12), 27729–27749.

Lockner, D., Walsh, J., & Byerlee, J. (1977). Changes in seismic velocity and attenuation during deformation of granite. *Journal of Geophysical Research*, *82*(33), 5374–5378.

Macdonald, A., & Fyfe, W. (1985). Rate of serpentinization in seafloor environments. *Tectonophysics*, *116*(1-2), 123–135.

Manning, C. E., Weston, P. E., & Mahon, K. I. (1996). Rapid high-temperature metamorphism of east pacific rise gabbros from hess deep. *Earth and Planetary Science Letters*, *144*(1-2), 123–132.

McKenzie, D., Jackson, J., & Priestley, K. (2005). Thermal structure of oceanic and continental lithosphere. *Earth and Planetary Science Letters*, *233*(3-4), 337–349.

Michibayashi, K., Hirose, T., Nozaka, T., Harigane, Y., Escartin, J., Delius, H., ... Ohara, Y. (2008). Hydration due to high-t brittle failure within in situ oceanic crust, 30 n mid-atlantic ridge. *Earth and Planetary Science Letters*, *275*(3-4), 348–354.

Moore, D. E., & Lockner, D. A. (2004). Crystallographic controls on the frictional behavior of dry and water-saturated sheet structure minerals. *Journal of Geophysical Research: Solid Earth*, *109*(B3).

Naif, S., Key, K., Constable, S., & Evans, R. L. (2015). Water-rich bending faults at the m iddle a merica t rench. *Geochemistry, Geophysics, Geosystems*, *16*(8), 2582–2597.

Nicolas, A., Fortin, J., Regnet, J., Dimanov, A., & Guéguen, Y. (2016). Brittle and semi-brittle behaviours of a carbonate rock: influence of water and temperature. *Geophysical Journal International*, *206*(1), 438–456.

Nozaka, T., & Fryer, P. (2011). Alteration of the oceanic lower crust at a slow-spreading axis: Insight from vein-related zoned halos in olivine gabbro from atlantis massif, mid-atlantic ridge. *Journal of Petrology*, *52*(4), 643–664.

Nozaka, T., Wintsch, R. P., & Meyer, R. (2017). Serpentinization of olivine in troctolites and olivine gabbros from the hess deep rift. *Lithos*, *282*, 201–214.

Okazaki, K., & Hirth, G. (2020). Deformation of mafic schists from subducted oceanic crust at high pressure and temperature conditions. *Tectonophysics*, *774*, 228217.

Paterson, M. S., & Wong, T.-f. (2005). *Experimental rock deformation-the brittle field*. Springer Science & Business Media.

Ranero, C. R., Morgan, J. P., McIntosh, K., & Reichert, C. (2003). Bending-related faulting and mantle serpentinization at the middle america trench. *Nature*, *425*(6956), 367–373.

Sayers, C. M., & Kachanov, M. (1995). Microcrack-induced elastic wave anisotropy of brittle rocks. *Journal of Geophysical Research: Solid Earth*, *100*(B3), 4149–4156.

Scholz, C. H. (2019). *The mechanics of earthquakes and faulting*. Cambridge university press.

Scholz, C. H., Sykes, L. R., & Aggarwal, Y. P. (1973). Earthquake prediction: a physical basis. *Science*, *181*(4102), 803–810.

Schubnel, A., Benson, P. M., Thompson, B. D., Hazzard, J. F., & Young, R. P. (2006). Quantifying damage, saturation and anisotropy in cracked rocks by inverting elastic wave velocities. In *Rock damage and fluid transport, part i* (pp. 947–973). Springer.

Shillington, D. J., Bécel, A., Nedimović, M. R., Kuehn, H., Webb, S. C., Abers, G. A., ... Mattei-Salicrup, G. A. (2015). Link between plate fabric, hydration and subduction zone seismicity in alaska. *Nature Geoscience*, *8*(12), 961–964.

Suhr, G., Hellebrand, E., Johnson, K., & Brunelli, D. (2008). Stacked gabbro units and intervening mantle: A detailed look at a section of iodp leg 305, hole u1309d. *Geochemistry, Geophysics, Geosystems*, *9*(10).

Tullis, T. E., Horowitz, F. G., & Tullis, J. (1991). Flow laws of polyphase aggregates from end-member flow laws. *Journal of Geophysical Research: Solid Earth*, *96*(B5), 8081–8096.

Van Avendonk, H. J., Holbrook, W. S., Lizarralde, D., & Denyer, P. (2011). Structure and serpentinization of the subducting cocos plate offshore nicaragua and costa rica. *Geochemistry, Geophysics, Geosystems*, *12*(6).

Wan, K., Lin, J., Xia, S., Sun, J., Xu, M., Yang, H., ... Xu, H. (2019). Deep seismic structure across the southernmost mariana trench: Implications for arc rifting and plate hydration. *Journal of Geophysical Research: Solid Earth*, *124*(5), 4710–4727.

Wang, Q., Bagdassarov, N., & Ji, S. (2013). The moho as a transition zone: A revisit from seismic and electrical properties of minerals and rocks. *Tectonophysics*, *609*, 395–422.

Yoshida, K., Okamoto, A., Shimizu, H., Oyanagi, R., Tsuchiya, N., & Oman Drilling Project Phase 2 Science Party. (n.d.). Fluid infiltration through oceanic lower crust in response to reaction-induced fracturing: Insights from serpentinized troctolite and numerical models. *Journal of Geophysical Research: Solid Earth*, e2020JB020268.

Zaima, K., & Katayama, I. (2018). Evolution of elastic wave velocities and amplitudes during triaxial deformation of aji granite under dry and water-saturated conditions. *Journal of Geophysical Research: Solid Earth*, *123*(11), 9601–9614.